Evaluation of Algorithms for Orientation Invariant Inertial Gait Matching

Ravichandran Subramanian, *Student Member, IEEE*, and Sudeep Sarkar, *Fellow, IEEE*

***Abstract*— With the prevalent use of smart phones in sensitive applications, unobtrusive methods for continuously verifying the identity of the user have become critical. The embedded inertial sensors in these devices provide an opportunity to develop authentication processes based on behavioral biometrics such as gait. However, one major obstacle is that the orientation of the device relative to the user is hard to control and difficult to determine reliably. This paper presents five methods: magnitude (MAG), principal component analysis (PCA), vector cross product (VCP), reduced gait dynamics image (rGDI), and Kabsch alignment (KAB) that make the authentication process independent of device orientation and hence improve the performance. The five methods are evaluated and compared on two large, publicly available, inertial gait datasets. The baseline (orientation dependent) average equal error rate (EER) when the device was freely oriented is 26.4%. The MAG, PCA, VCP, and rGDI methods reduce the average EER to approximately 23%. The Kabsch (KAB) method is more effective and reduces the average EER to 20.2%.**

***Index Terms*— Biometrics, gait, inertial sensors, orientation invariance, wearable sensors.**

I. Introduction

AUTHENTICATION mechanisms based on behavioral biometrics have been an active area of research for the past several decades. Behavioral biometrics, as the name implies, is based on the characteristic manner in which an individual performs a natural action. Examples of such actions used in biometric authentication are, typing on physical or virtual keyboards (keystroke dynamics) [40], mouse movement [32], eye movements (saccades) [12] and gait [14], [30].

Each of the above behaviors has its characteristic strengths and weaknesses depending on the context of application. When the subject is using a laptop or desktop computer, the keystroke dynamics and mouse movement characteristics are appropriate. If the computer has an integrated camera, the lighting is favorable and the subject's face/eyes are not obscured, facial recognition or saccade patterns can be used for authentication. Gait is the behavior of choice for biometric authentication when the subject is walking or running.

Manuscript received January 27, 2018; revised May 11, 2018; accepted June 7, 2018. Date of publication June 25, 2018; date of current version August 2, 2018. The associate editor coordinating the review of this manuscript and approving it for publication was Prof. Yunhong Wang. *(Corresponding author: Ravichandran Subramanian.)*

The authors are with the Department of Computer Science and Engineering, University of South Florida, Tampa, FL 33620 USA (e-mail: rsubramanian@usf.edu; sarkar@usf.edu).

Color versions of one or more of the figures in this paper are available online at http://ieeexplore.ieee.org.

Digital Object Identifier 10.1109/TIFS.2018.2850032

Patel *et al.* [28] discuss the need for continuous authentication on mobile devices and present some of the current research and challenges in this area. One authentication modality that is well suited for continuous authentication is gait based authentication using inertial sensors.

One of the serious issues in using smartphones with embedded inertial sensors for gait based authentication is that, it is not always practical to control or determine the orientation of the device relative to the user. The inertial signals are recorded in a coordinate system relative to the smartphone. But for biometric purposes, the gait dynamics need to be represented in a coordinate system relative to the user. There is no reliable way to transform from one coordinate system to the other without knowing how the device is oriented relative to the user. Since the gallery (reference signal) and the probe (test signal) for a user are essentially collected at different times, it is highly unlikely that the device remains in the same orientation relative to the user at both instances. To be suitable for real world applications, inertial gait based authentication systems need to include effective methods to deal with this change in orientation.

In this paper we introduce two new methods to address orientation change, one based on Principal Component Analysis (PCA) and the other based on Vector Cross Product (VCP). We also present an optimization of a previously published method [47] based on Gait Dynamics Image (GDI). These are compared against a method based on Kabsch alignment from [37], a simple magnitude based representation widely used by other researchers and a baseline method of no correction at all. The comparison is based on the performance of these methods on two of the largest publicly available inertial gait datasets. When the phone orientation is unconstrained, the orientation independent methods show a 13% to 23% increase in performance relative to the orientation dependent baseline method.

II. Gait Modalities

There are several ways in which the gait of the subject can be captured, each with its own merits and shortfalls. One approach uses sensors on the walking surface. These sensors record the force pattern exerted by the feet and gait features are derived based on these patterns. This technique has been most useful in the medical context for characterizing gait for rehabilitation and diagnostics. There has been limited research done using this method for authentication [34], [43], [19]. Since the sensors can cover only a limited area, this technique

has limited applicability for authentication for general scenarios. For instance it could be used for access control between passages [41]. One significant covariate that is expected to cause problem with this modality is the weight of additional objects carried by the subject. This modality is expected to be less sensitive to the clothing, provided they are not restrictive enough to affect the gait. Identification rates of higher than 90% have been reported on several small databases [38], [18], [45]. Another interesting use of gait for authentication is using a pair of smart socks that can measure acceleration and ground contact forces [27].

Imaging based approaches have been the most active area of research for gait based authentication. The main reasons for this are the maturity of various camera technologies (resolution, robustness) and the availability of different modalities (RGB/color, Infrared, depth). One advantage of this approach is that it can be done covertly. However, there are various covariates that cause issues with this technique. One can address the dependence of camera view angle by using multiple views. There is also dependence on shoe type, walking surface and whether or not the subject is carrying something. Identification rates of above 90% have been reported on various large datasets (100 subjects or more) [31]. However performance on few covariates such as surface type and elapsed time have saturated below 60% and 30% respectively. There are several large databases available for evaluating the performance of authentication methods. SOTON HID Gait dataset [33] contains 115 subjects collected under controlled conditions indoors and also some outdoor sequences. The USF Human ID dataset [30] contains 122 subjects collected outdoors with 2 cameras and various covariates such as carry condition, shoe type, walking surface and elapsed time. It is still the largest outdoor gait dataset. CASIA-B dataset [44] contains sequences with changes in view angle, clothing and carry condition. CASIA-C dataset [39] has 153 subjects, walking at different speeds, captured by night vision (infrared) cameras. TUM-GAID dataset [9] is a multi-modal dataset with audio, grayscale image and depth images of 305 subjects. The OU-ISIR large population dataset [11] contains more than 4000 subjects spanning a wide range of ages captured in a controlled indoor environment with 2 cameras.

Imaging based approaches are not practical in all situations. For instance, in a secure complex with multiple buildings, the camera based system could be used in entryways and perimeter. The lighting and camera angles can be controlled in these areas for optimal performance of an image based gait authentication system. It would be uneconomical to place cameras to cover the pathways between the buildings and tailor the environment for image based gait authentication. In such situations an inertial sensor based gait authentication system is the ideal solution because it is co-located with the user.

There has been considerable interest in securing phones over the past 15 years due to the increasing utility and capability of smartphones. In terms of their utility, smartphones are used in a variety of sensitive contexts, such as financial transactions, accessing medical information, company email communications etc. In terms of capability, a wide variety of sensors such as high resolution cameras, fingerprint readers, inertial sensors (accelerometer and gyroscopes) have become standard features even in the cheapest of smartphones. The use of smartphones in security sensitive contexts requires reliable authentication methods, beyond the initial login, even when the phone is being carried in the pocket or holster. For example the phone could be running applications that receive sensitive audio and transmitting to the user over earphones or enable some location based functionality such as opening doors to a secure facility. The ability of the device to verify the user without distracting the user is a requirement in many situations and an added convenience in others. Modalities such as face, fingerprint, and passwords are not suitable for continuous or frequent authentication due to their obtrusive nature. Continuous authentication based on gait as captured by the accelerometer and gyroscope in mobile devices offers an excellent mechanism in these cases [42]. Other use cases can arise in high security scenarios where the security of the device itself is at stake, such as in the battlefield when you want a device to lock itself (or even self destruct) anytime it thinks it is the hands or is being carried by the enemy. Parts of this paper are based on research conducted in response to the US DARPA Active Authentication program that foresaw the need for this kind of technology. Another scenario is in healthcare setting where privacy is important and many of the devices with patient information in them are going mobile. You would like a tablet to lock itself if it suspects that a non-user is carrying it away. We discuss previous works in inertial gait based authentication in more detail in the next section.

III. Previous Research in Inertial Gait

Initial research using inertial sensors for gait recognition was performed by Ailisto *et al.* [1] and Mantyjarvi *et al.* [16]. The study used a free standing accelerometer attached to the back of the hip in fixed position/orientation. Based on 36 subjects they achieved EER's in the 6% to 7% range using similarity methods. More recently, Dehzangi *et al.* [3] use a body area network of 5 sensors on 10 subjects and report identification accuracy of 93% to 97% using convolutional neural networks. Nguyen *et al.* [24] achieve an EER of about 12% on the OU-ISIR-2 Inertial Gait Database [22] using convolutional neural net for classification. Sprager and Juric [36] present an extensive review of inertial sensor based gait recognition.

Currently very little research has been published to address the problem with change in orientation of the device. This is probably due to the fact that very little data has been collected with no restriction on device orientation. Most datasets are collected with inertial sensors that are placed at a predetermined fixed orientation with respect to the user. The ZJU-GaitAcc database [46] is a large database collected using 175 subjects with 5 accelerometers in fixed orientation located at different parts of the body. This dataset is more suitable for investigating performance sensitivity to sensor location than sensor orientation. The OU-ISIR-2 Inertial Gait Database [22] is collected with fixed orientation of multiple sensors around the waist. Since all the sensors are around the waist, they are

expected to record similar gait dynamics compared to sensors located at different parts of the body (for example upper arm and thigh). In spite of each sensor being in a fixed orientation, there is an orientation difference between sensor pairs. Thus the dataset can be used to analyze orientation variation. The McGill gait dataset [5] and our USF-PDA dataset[1] [37] are the only publicly available datasets with no restriction on phone orientation known at this time.

Several strategies described below have been used to deal with change in orientation.

A. Extend Gallery With Artificial Data

In [10], the orientation problem is addressed by generating pseudo galleries at 26 different orientations of the device at 15° steps about each axis. This does not account for all possible orientations of the device. They report an accuracy of about 85% for normal walk. However the experiment uses only 2 subjects. The generation of artificial data may not be accurate due to calibration issues and it overloads the similarity computation process.

B. Use Orientation Agnostic Features

In this category, new features which are insensitive to the device orientation are generated from the original signals. The same process is applied to the gallery and probe independently. An example of this method is to use only the magnitude of the signal, as presented in [5] and [26]. However, this ignores rich gait dynamics information captured in 3D that can provide discriminative information between subjects. Reported error rates are high with this approach; EERs of about 15% for *same day* and about 55% for *cross day* evaluation have been reported in [5]. This conforms with our own experience.

Another such method presented in [47], deals with orientation in time domain by creating a matrix of rotation invariant features for each signal. These features are the inner product and the cosine of pairs time series data at different time lags. Inner product and the cosines are computed with respect to a chosen signal vector in the time series. Thus, the 3D signal sequence is transformed into a scalar signal sequence that is invariant to the rotation of the signal. It presents accuracies in the 85% range for *same day* and 65% range for *cross day* on the McGill dataset [5].

Frequency domain methods also can be used to address the orientation issue as in [15]. It gets only less than 50% accuracy. There is some evidence that frequency domain features perform poorly compared to time domain features [16], [29] in general.

C. Rotate Signals to a Canonical Orientation

The gallery and probe signals are rotated independently to some canonical orientation. Cola *et al.* [2] and Hoang *et al.* [7], [8] have transformed the signals into two components, one in the vertical direction and the other in the terrestrial plane. While this is better than the scalar magnitude, it conflates the gait dynamics in the forward and lateral directions. Cola *et al.* [2] report EERs varying from 14.8% to 9.8% depending on the fraction of data used for training on realistic data from 6 subjects. Hoang *et al.* [7] report same day EER of 2.45% on a dataset of 38 subjects.

[1] Available at https://github.com/ravisub/USF-Inertial-Gait

D. Rotate One Signal to Match the Other

In these methods, an optimal rotation (defined by some cost function) is computed based on both the gallery and probe and applied to one of the signals. A method based on the Kabsch alignment has been used in [37] to minimize the L^2 norm of errors to find a rotation transformation of the probes to the gallery. A dynamic programming based method that uses Levenberg-Marquardt least squares algorithm to maximize the normalized cross-correlation is presented in [23]. On a small dataset of 47 subjects it reports EERs ranging from 1.7% to 4.6%.

IV. Generalized Framework for Inertial Gait Authentication

The inputs to the inertial gait authentication algorithm are two time-series of sensor data, one corresponding to the gallery and the other to the probe. The sensor data is made of 3-D acceleration vector sequence (gravity having been removed) $\{\ddot{\mathbf{x}}(i)|i = 0 : n-1\}$, and 3-D gyroscope vector sequence $\{\dot{\boldsymbol{\theta}}(i)|i = 0 : n-1\}$. The authentication process consists of three steps: gait cycle splitting, feature generation, and matching.

A. Cycle Splitting

The accelerometer and gyroscope signals are split into smaller chunks, each representing one complete gait cycle. To split the signals into gait cycles, first the gait cycle period is estimated using autocorrelation of the 3D accelerometer signal. Then peaks that are approximately estimated period apart are located in the acceleration magnitude signal. The peak pairs correspond to overlapping gait cycles alternately starting with each foot. The timestamps corresponding to the peaks are used to extract accelerometer and gyroscope signals representing the gait cycles. This process is described in more detail in [37].

Because the resulting cycles are of varying time duration, they contain different numbers of samples. To facilitate easy comparison, each gait cycle is resampled using linear interpolation, to produce ($m = 102$) samples. We denote these resampled data by $3 \times m$ matrices $\ddot{\mathbf{X}} = \left[\ddot{\mathbf{x}}(0), \cdots, \hat{\ddot{\mathbf{x}}}(m-1)\right]$ and $\dot{\Theta} = \left[\dot{\boldsymbol{\theta}}(0), \cdots, \dot{\boldsymbol{\theta}}(m-1)\right]$ corresponding to the accelerometer and gyroscope measurements, where each column represents the 3D acceleration/rotation rate at an instant of time.

B. Feature Generation

The resampled data from the gallery and probe is used to generate features that are independent of sensor orientation. One gallery cycle and one probe cycle, collected with different sensor orientation for the same subject are presented in Figure 1. If they were to be compared as such, the resulting

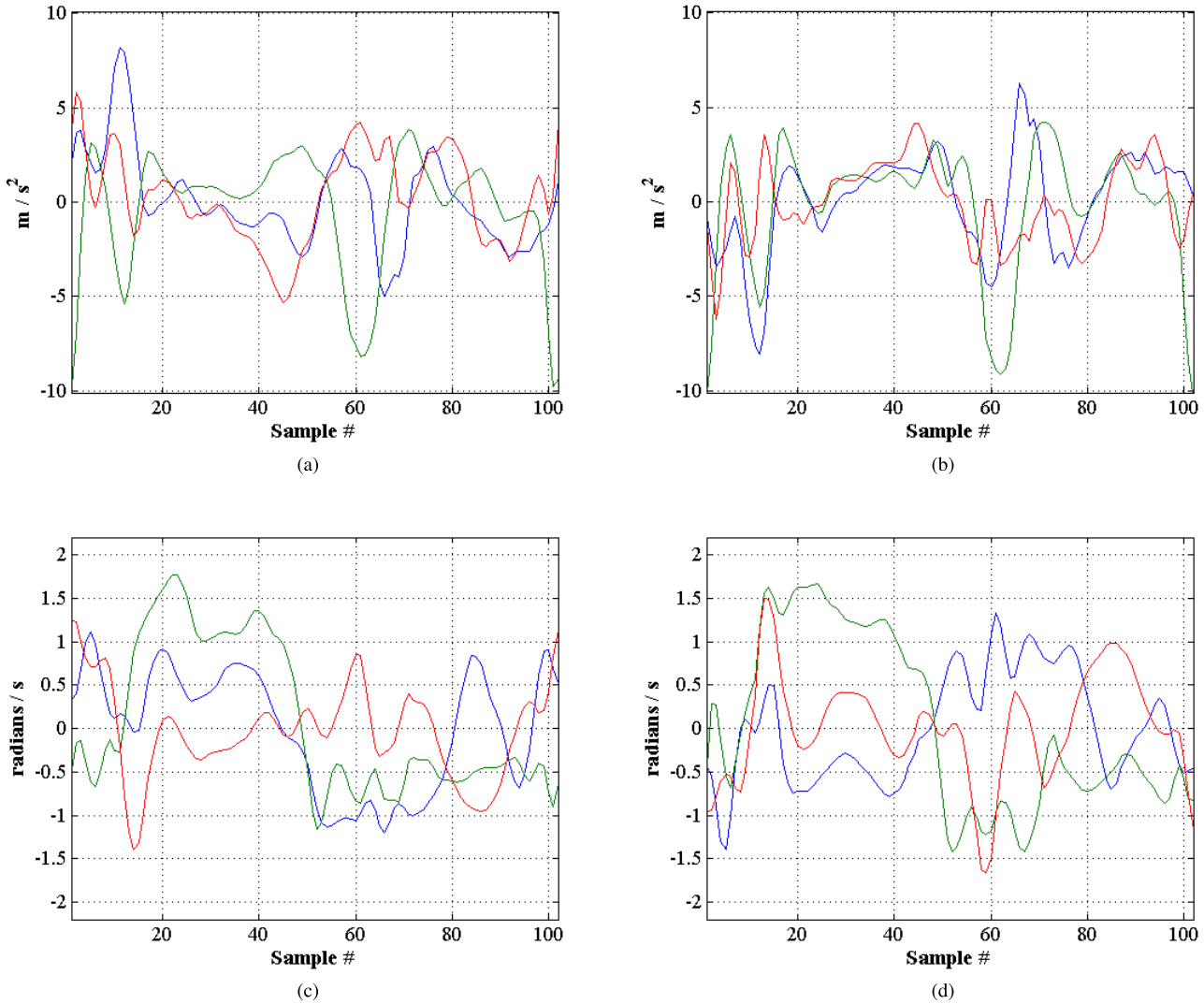

Fig. 1. The accelerometer and gyroscope signals corresponding to one gait cycle of the same subject are shown here. The blue, green and red plots respectively represent the X, Y and Z components of the signal in the device coordinates. (a) Accelerometer signal for one gait cycle from the gallery. (b) Accelerometer signal for one gait cycle from the probe. (c) Gyroscope signal for one gait cycle from the gallery. (d) Gyroscope signal for one gait cycle from the probe. While the Y (green) component is similar between the gallery and probe, the X (blue) and Z (red) components are inverted between the gallery and probe. This indicates a 180° rotation about the Y axis between the gallery and probe.

match would be poor due to the orientation difference. We describe the five methods considered in this paper, along with figures showing the orientation independent features generated by them in this section.

1) Magnitude (MAG): The magnitude is the L^2 norm of each 3D vector in the time series.

$$m(i) = \sqrt{s_x(i)^2 + s_y(i)^2 + s_z(i)^2} \tag{1}$$

where s_x, s_y and s_z are the 3D components of the accelerometer or gyroscope signal. An illustration of the magnitudes of accelerometer and gyroscope signals corresponding to one gait cycle from the gallery and probe of the same subject is shown in Figure 2.

2) Principal Component Analysis (PCA): In this method the rotation matrix $\mathbf{R}$ is the matrix of eigenvectors of the covariance matrix of the mean subtracted acceleration time series $\ddot{\mathbf{X}}$. The same rotation matrix is used to align both the accelerometer and gyroscope signals after subtracting respective means. Since it is possible for the resulting matrix to include a reflection of a pair of axes, additional versions of the rotated gallery data are generated to include the 3 possible reflections. The aligned version of the probe is generated in a similar manner and compared against all the 4 versions of the gallery data. The PCA aligned signals of gallery and probe of the same subject are shown in Figure 3.

3) Vector Cross Product (VCP): In this method the rotation matrix $\mathbf{R}$ is designed to place the X-axis along the mean acceleration vector $\bar{\ddot{\mathbf{X}}}$, and the Y axis perpendicular to both the mean acceleration vector $\bar{\ddot{\mathbf{X}}}$ and the mean gyroscope vector $\bar{\dot{\mathbf{\Theta}}}$. The uncertainty in the rotation matrix increases with small values of the mean vectors. Since full gait cycle typically produces small values for the means, the mean vectors $\bar{\ddot{\mathbf{X}}}$ and $\bar{\dot{\mathbf{\Theta}}}$ are computed using only the first half of the samples in the time-series.

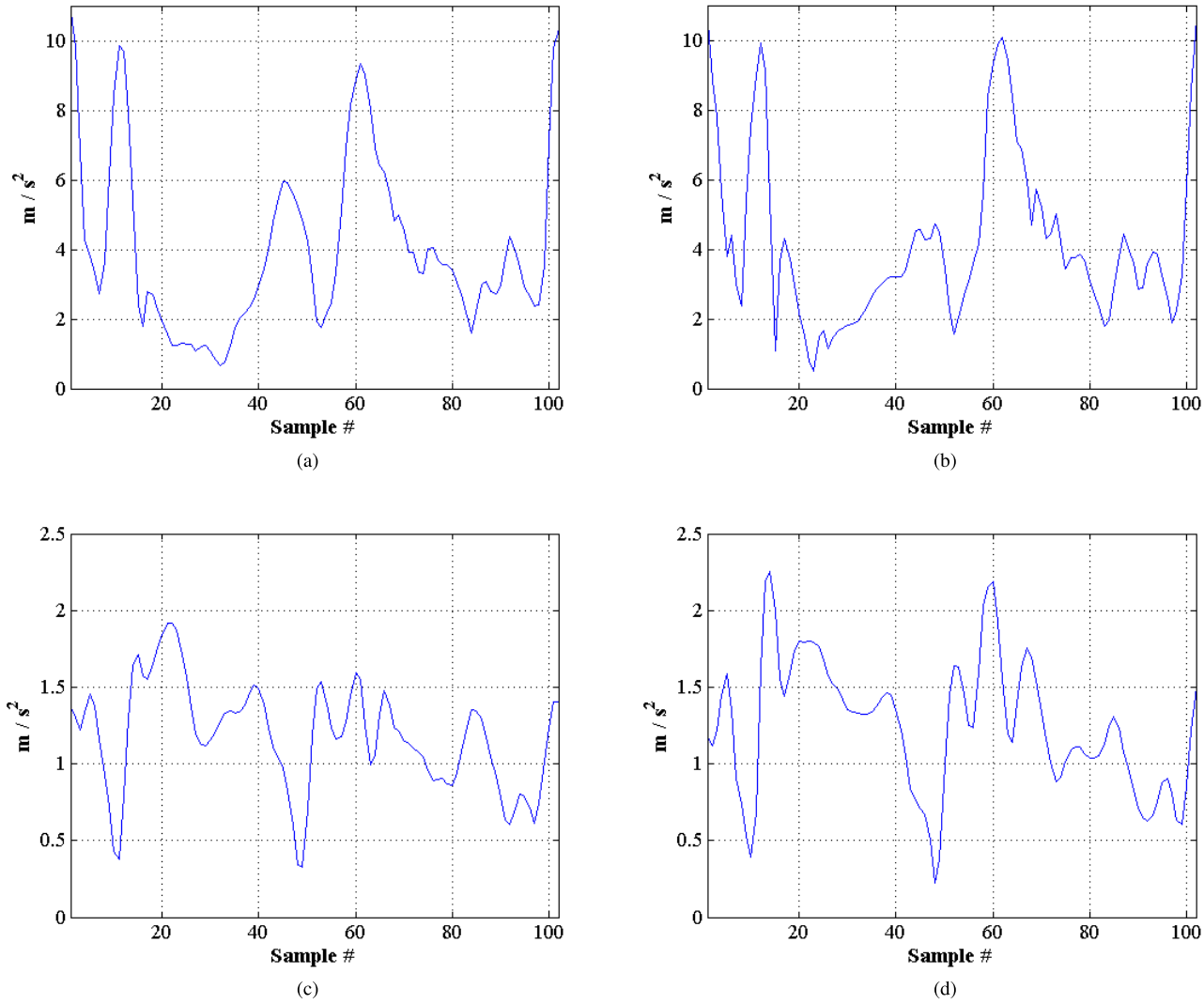

Fig. 2. The magnitudes of the accelerometer and gyroscope signals shown in Fig. 1 are shown here. (a) Magnitude of the accelerometer signal for one gait cycle from the gallery. (b) Magnitude of the accelerometer signal for one gait cycle from the probe. (c) Magnitude of the gyroscope signal for one gait cycle from the gallery. (d) Magnitude of the gyroscope signal for one gait cycle from the probe. Based on the magnitude representation, the accelerometer signals are similar between the gallery and probe and the gyroscope signal is similar between the gallery and probe. The rotation invariance has been achieved at the cost of 3 dimensional signals being reduced to one dimension.

If $\mathbf{u_x}$ is the unit vector along the direction of mean acceleration and $\mathbf{u}_\theta$ is the unit vector along the direction of the mean gyroscope, $\mathbf{R}$ is computed as follows:

$$\mathbf{u_1} = \mathbf{u_x} \tag{2}$$

$$\mathbf{u_2} = \mathbf{u_x} \times \mathbf{u}_\theta \tag{3}$$

$$\mathbf{u_3} = \mathbf{u_1} \times \mathbf{u_2} \tag{4}$$

$$\mathbf{R} = \begin{pmatrix} \mathbf{u_1}^T \\ \mathbf{u_2}^T \\ \mathbf{u_3}^T \end{pmatrix} \tag{5}$$

The VCP aligned signals of gallery and probe of the same subject are shown in Figure 4.

4) Reduced Gait Dynamics Image (rGDI): The idea that projection of one vector along another is invariant when the both the vectors are rotated together is used in [47] to generate rotation invariant representation of the acceleration and gyroscope time series in the form of the Gait Dynamics Image (GDI). The GDI is an arrangement of projections between all vector pairs in the time series. With 102 entries in the time series, there are 102 projections with zero stride (each vector with itself), there are 101 projections with a stride of 1 and in general $(102 - n)$ projections with a stride of n. This results in $\frac{102\times103}{2} = 5253$ entries in the full GDI. In the case of 3D vectors, projections along 3 independent axes completely determine the rotation and consequently the full GDI contains an excessive amount of redundant information. To reduce this redundancy, the *reduced GDI*, uses only strides 0 through 7. This results in 788 entries, which is only 15% of the full GDI entries. The rGDI features are shown in Figure 5.

5) Kabsch Alignment (KAB): In this method the probe cycle is rotated such that the L^2 (Frobenius) norm of the error between the rotated version of the probe cycle and the gallery cycle is minimized,

$$\hat{\mathbf{R}} = \arg\min_{\mathbf{R}} \ \|\mathbf{Y}_g - \mathbf{R}\mathbf{Y}_p\|_2 \tag{6}$$

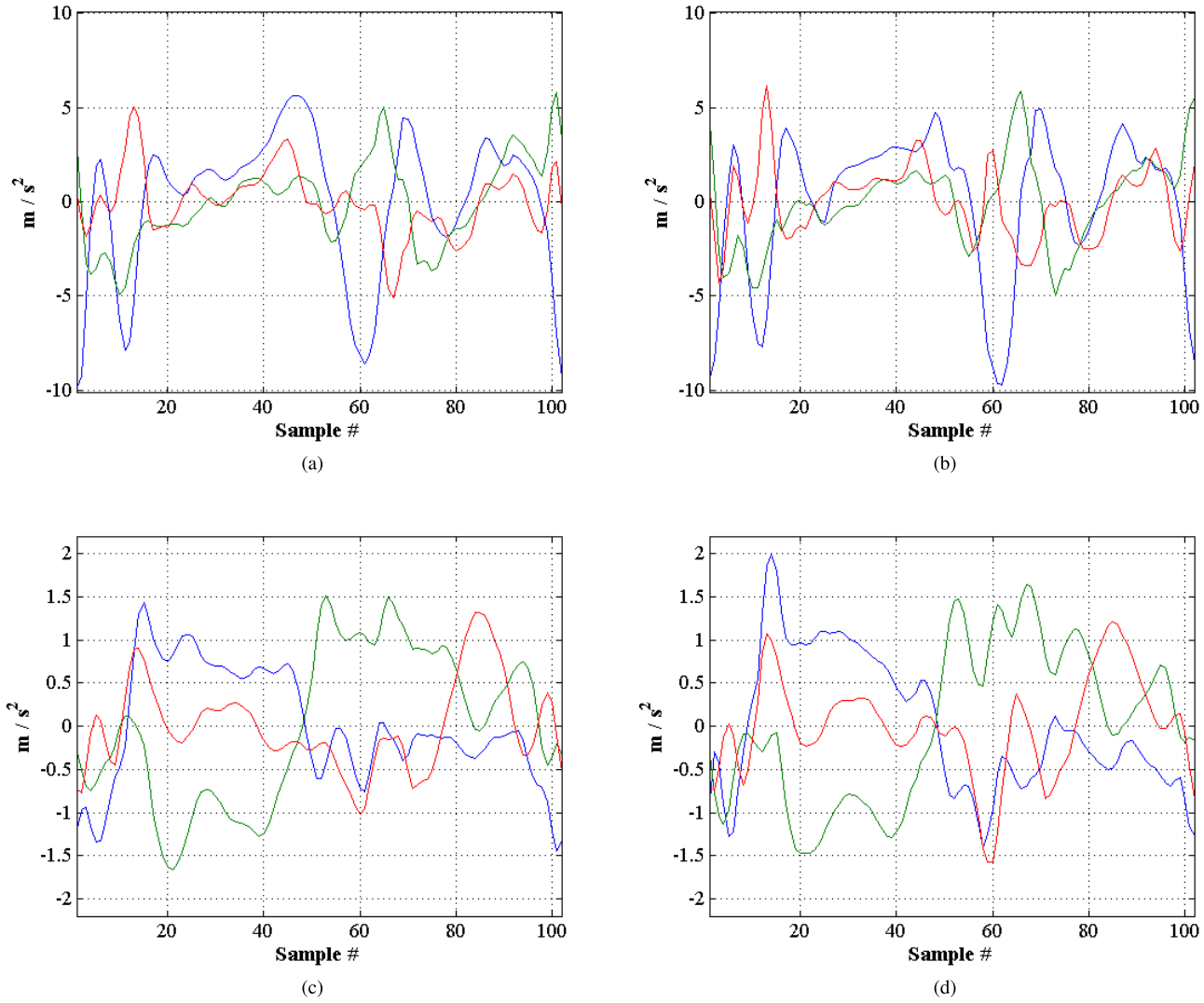

Fig. 3. The Principal components of the accelerometer and gyroscope signals shown in Fig. 1 are shown here. . The blue, green and red plots respectively represent the first, second and third principal components of the signal. (a) Accelerometer signal for one gait cycle from the gallery. (b) Accelerometer signal for one gait cycle from the probe. (c) Gyroscope signal for one gait cycle from the gallery. (d) Gyroscope signal for one gait cycle from the probe. The gallery and probe signals show a greater similarity in the principal component transformed form.

where $\mathbf{Y}$ is the concatenation of the accelerometer time series $\dot{\mathbf{X}}$ and the gyroscope time series $\dot{\mathbf{\Theta}}$. This is equivalent to minimizing the trace of $\left(\mathbf{Y}_g - \mathbf{R}\mathbf{Y}_p\right)^T \left(\mathbf{Y}_g - \mathbf{R}\mathbf{Y}_p\right)$. A similar problem was solved by Kabsch [13] in the context of crystallography.

The solution can be constructed from the singular value decomposition (SVD) of the 3×3 matrix $\mathbf{Y_g Y_p}^T$ given by $\mathbf{U}\Lambda\mathbf{V^T}$. We resolve the ambiguity of the rotation matrix in terms of a right-handed coordinate system by setting the determinant sign appropriately, using $s = \text{sign}(\det(\mathbf{VU}^T))$. Using this, our optimal rotation matrix is given by

$$\hat{\mathbf{R}} = \mathbf{V} \begin{pmatrix} 1 & 0 & 0 \\ 0 & 1 & 0 \\ 0 & 0 & s \end{pmatrix} \mathbf{U}^T \tag{7}$$

An illustration of the effect of rotation alignment of the probe signals is shown in Figure 6. In this case, the probe had the phone rotated about its Y axis, which is fixed after alignment.

C. Matching

The features are arranged into 1-dimensional vectors $\mathbf{S_g}$ and $\mathbf{S_p}$ representing one gallery cycle and one probe cycle respectively. The gallery and probe features are compared using Tanimoto similarity measure. The Tanimoto similarity between $\mathbf{S_g}$ and $\mathbf{S_p}$ is computed as:

$$T(\mathbf{S_g}, \mathbf{S_p}) = \frac{\mathbf{S_g} \circ \mathbf{S_p}}{\mathbf{S_g} \circ \mathbf{S_g} + \mathbf{S_p} \circ \mathbf{S_p} - \mathbf{S_g} \circ \mathbf{S_p}} \tag{8}$$

where the operation $\mathbf{A} \circ \mathbf{B}$ denotes the sum of the entry wise multiplication of the matrices, i.e. $\sum_i \sum_j A_{ij} B_{ij}$. For signals that are similar, the value of this measure will be close to 1 and less if they are dissimilar.

We compared the performance of different similarity measures such as Tanimoto, Cosine and Normalized Cross Correlation (NCC) on a few experiments. As seen in Table I the relative variation EERs of the similarity measures is about

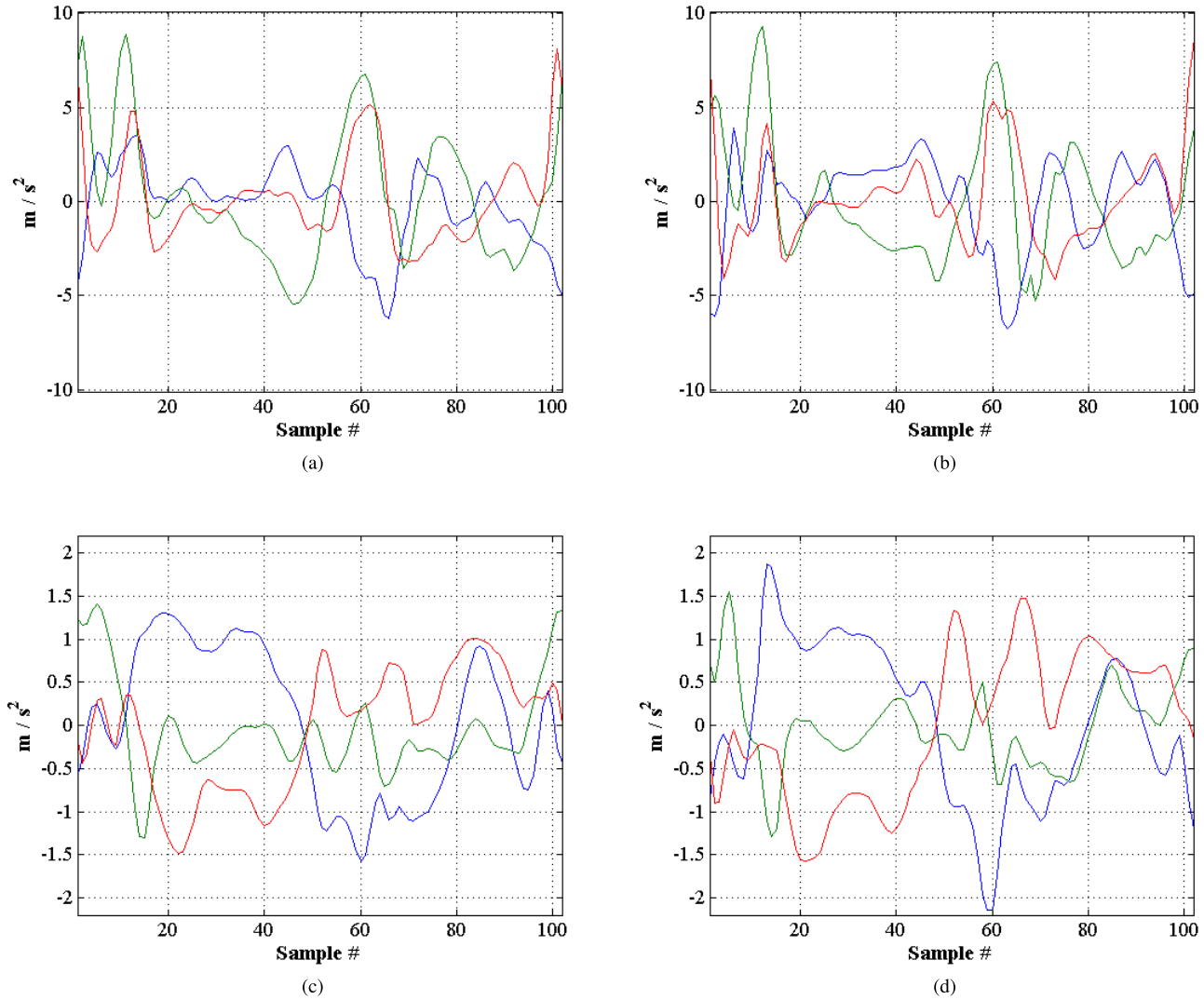

Fig. 4. The vector cross product (VCP) transformation of the accelerometer and gyroscope signals shown in Fig. 1 are shown here. The blue, green and red plots respectively represent the X, Y and Z components of the signal in the transformed coordinate system. (a) Accelerometer signal for one gait cycle from the gallery. (b) Accelerometer signal for one gait cycle from the probe. (c) Gyroscope signal for one gait cycle from the gallery. (d) Gyroscope signal for one gait cycle from the probe. The gallery and probe signals show a greater similarity in the VCP transformed form.

TABLE I

EQUAL ERROR RATES (EER) FROM EVALUATION OF TANIMOTO SIMILARITY, COSINE SIMILARITY AND NORMALIZED CROSS CORRELATION (NCC) ON TWO OF THE EXPERIMENTS, USING KABSCH BASED METHOD FOR ORIENTATION INVARIANCE. THE EXPERIMENTS USED GALLERY AND PROBES FROM SAME DAY, WITH REPOSITIONING OF THE DEVICE BETWEEN GALLERY AND PROBE COLLECTION. THE SIMILARITY MEASURES PRODUCE SIMILAR EERS, WITH TANIMOTO GIVING THE BEST PERFORMANCE

Experiment	Description	Tanimoto	Cosine	NCC
3	Holster	14.9%	15.3%	15.1%
4	Pocket	15.9%	16.6%	16.4%

4%, but Tanimoto similarity yields the lowest EER. So we use Tanimoto similarity for all experiments.

V. DATASETS

We compare the performance of the above rotation invariant methods on two of the largest publicly available inertial gait datasets: USF-PDA dataset and the OU-ISIR-2 Inertial Gait dataset.

A. USF-PDA Dataset

The Placement, Days and Activities (PDA) dataset [37] was collected from 101 subjects at University of South Florida in 2014 with the approval of Institutional Research Boards of USF and Air Force Research Laboratories (AFRL). The dataset covers different phone placements and activities performed by the subjects. Activities #1 - #12 were not gait related since the subject was not walking. During activities #13 - #18 shown in Table II, the subject walked with the phone at a specified home location (pocket / holster). For the gait related activities, the subject walked 3 times around the path (loop) shown in Figure 7. The phone was placed in the home location at the beginning of each activity. Activities #13 and #16 involved no repositioning of the phone. During the remaining activities the subject removed the phone from the home location and performed the specified phone

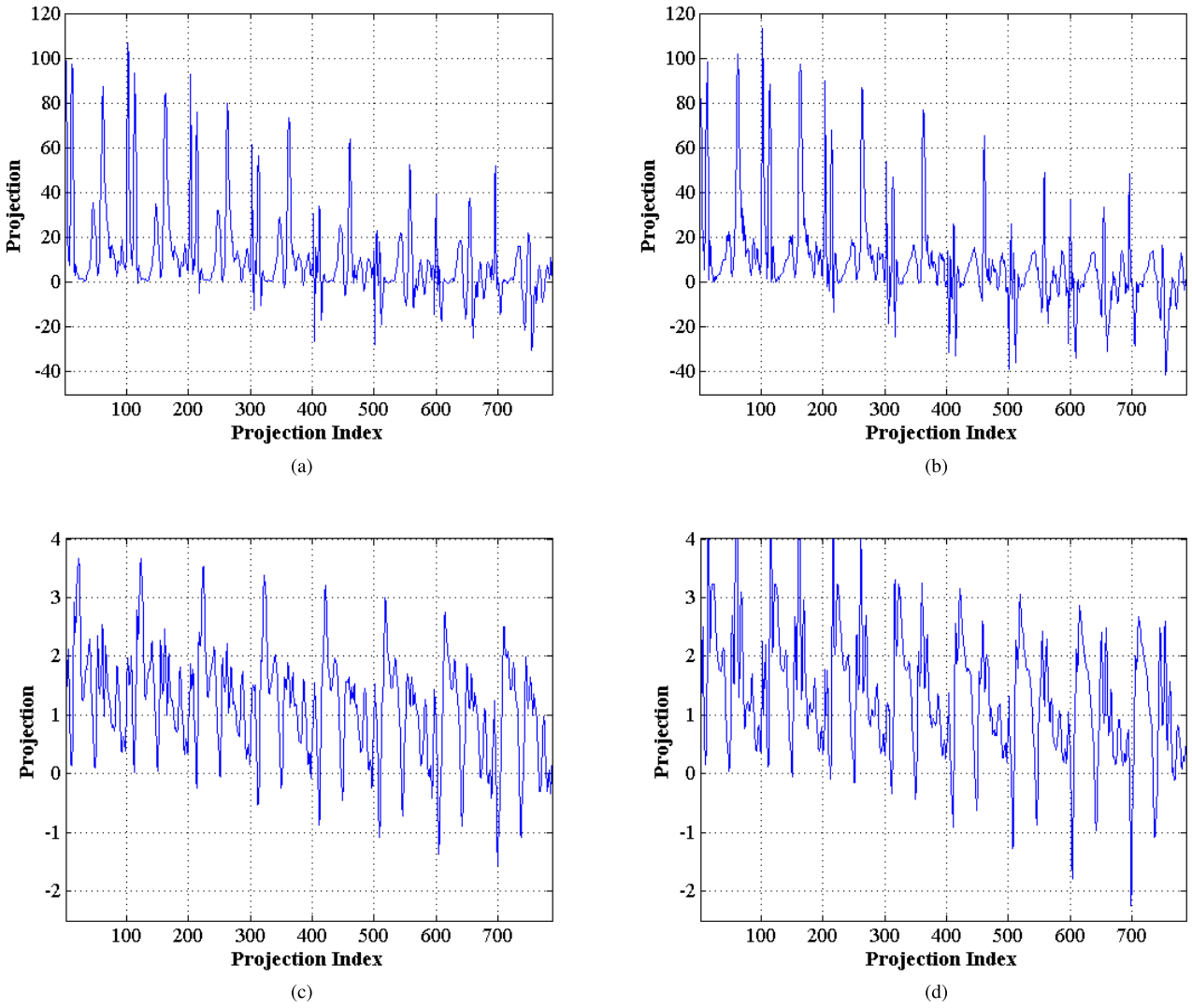

Fig. 5. The 788 features of the reduced Gait Dynamics Image (rGDI) corresponding to each of the accelerometer and gyroscope signals shown in Fig. 1 are shown here. (a) Accelerometer signal for one gait cycle from the gallery. (b) Accelerometer signal for one gait cycle from the probe. (c) Gyroscope signal for one gait cycle from the gallery. (d) Gyroscope signal for one gait cycle from the probe. The rGDI features of the gallery and probe signals show a great similarity.

TABLE II

THE 6 GAIT ACTIVITIES. *Home Location* IS THE LOCATION OF THE PHONE WHEN THE SUBJECT IS NOT USING IT. *Phone Action* IS THE MODE OF PHONE USAGE, IF ANY. NOTE THAT ACTIVITY IDS MATCH THOSE IN OUR DATABASE THAT INCLUDE NONGAIT ACTIVITIES (#1 - #12) WHICH ARE NOT PART OF THIS STUDY

Activity ID	Home location	Phone action
13	Pocket	NONE
14	Pocket	Talk
15	Pocket	Text
16	Holster	NONE
17	Holster	Talk
18	Holster	Text

action (Talk/Text) during the second time around the loop and replaced the phone in the home location, possibly in a different orientation.

Passage of time between gallery and probe data collection is an important covariate in biometrics. This also implicitly includes covariates such as clothing, footwear, mood and orientation of the phone relative to the user [17]. To study the performance of these covariates, data was collected a second time for 56 of these subjects, a few days after the first session.

B. OU-ISIR Inertial Gait Dataset

This data is fully described in [22]. Inertial gait data was collected from several hundred subjects using 3 IMUZ sensors (with triaxial accelerometer ans gyroscopes) and a Motorola smartphone with only a triaxial accelerometer. The IMUZ sensors were placed on the left, right and center (back) of the hip. The smartphone was colocated with the back IMUZ sensor. Data was collected during level, up slope and down slope walks. Each walk was performed twice. The data is divided into 2 subsets. The first subset OU-ISIR-1 contains automatically segmented level walk data from center IMUZ for 744 subjects. The second subset OU-ISIR-2 contains manually segmented data from all 3 IMUZs for all walks from 495 subjects.

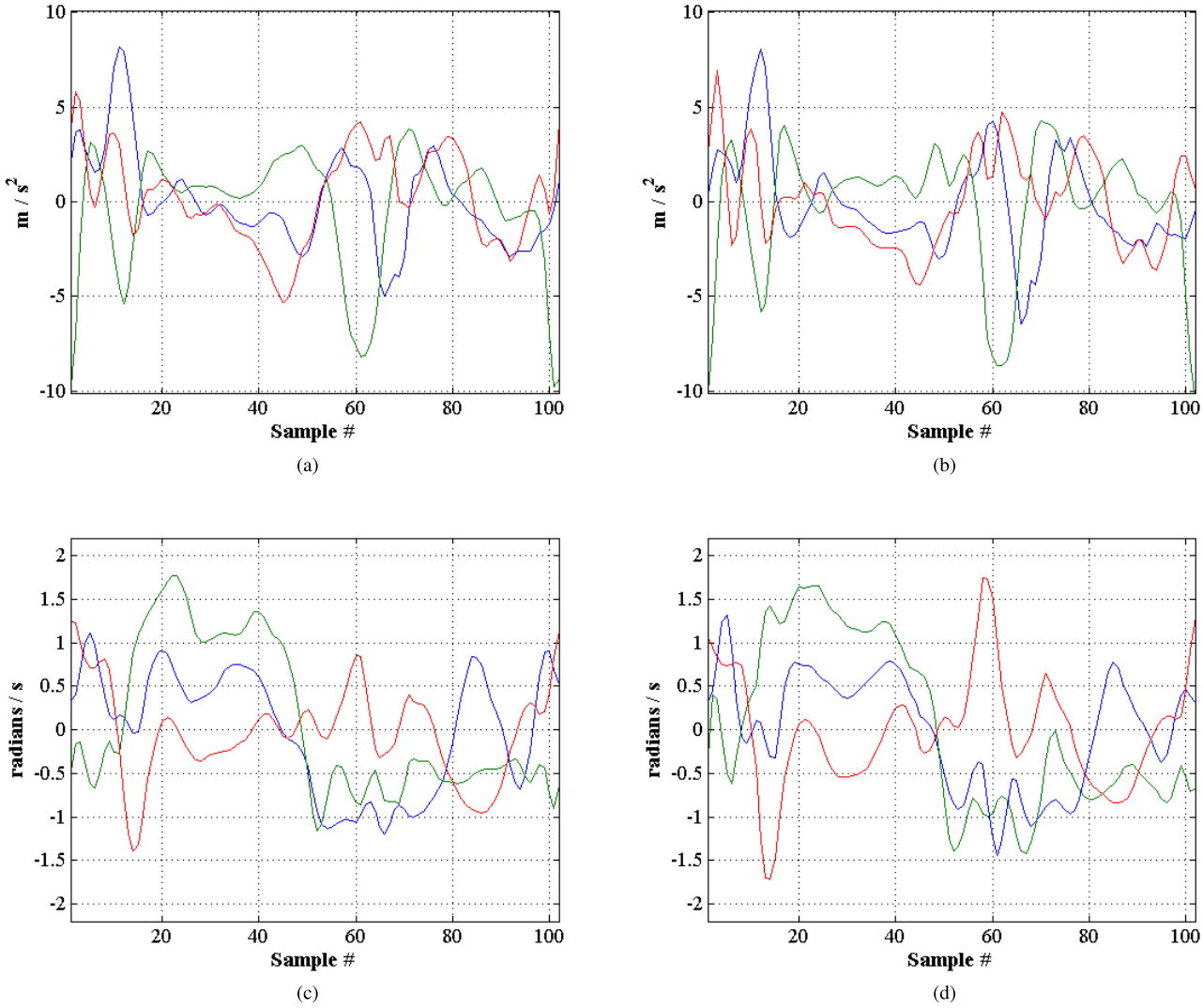

Fig. 6. The accelerometer and gyroscope signals of the gallery cycle shown in Fig. 1 and the Kabsch aligned accelerometer and gyroscope signals of the probe cycle shown in Fig. 1 are shown here. The blue, green and red plots respectively represent the X, Y and Z components of the signal. (a) Accelerometer signal for one gait cycle from the gallery. (b) Accelerometer signal for one gait cycle from the probe. (c) Gyroscope signal for one gait cycle from the gallery. (d) Gyroscope signal for one gait cycle from the probe. The gallery and probe signals show the alignment of the transformed probe coordinate system to the gallery coordinate system.

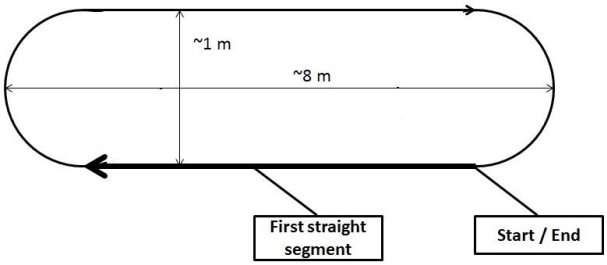

Fig. 7. Schematic of the walking path taken by subjects. The path was walked 3 times for each activity. The section of signal roughly corresponding to the first straight segment of the path from first loop in activities 13 and 16 was used as gallery.

VI. Experiments and Results

A. USF-PDA Dataset - Same Location

In these experiments, the gallery and probe come from activities that have the same home location for the phone. That is, probes from pocket activities are compared against pocket gallery and probes from holster activities are compared against holster gallery.

We designed six experiments to study algorithm performance by choosing gallery and probes with different characteristics. The galleries always came from activities that involved no phone action (13 or 16) from the first session for the subject. The gallery approximately corresponds to the first straight segment of the walk (see Figure 7) for these activities. The probes were formed from the remaining walking portion of activities 13 and 16, and the walk-only parts of remaining gait activities (14, 15, 17 and 18). For *same day* evaluation, probes came from the first session (same session as gallery). For *cross day* evaluation the probes came from the second session (different session than used for gallery). The probe portion of the data is split into 5 second segments to generate probes. The six experiments are as follows:

- Experiment 1 (Same day, Hoslter, No repositioning): For this experiment, both the gallery and probes are from activity 16 during first session. In this case, the phone orientation is not expected to change much between the gallery and probe collection due to it being in the holster.
- Experiment 2 (Same Day, Pocket, No repositioning): For this experiment, both the gallery and probes are from activity 13 during the first session. Here the phone was not repositioned between the gallery and probe collection.
- Experiment 3 (Same day, Holster, With repositioning): For this experiment, the gallery is from activity 16 of the first session and the probes are from activities 16, 17, and 18 of the first session. In this experiment, the phone is removed and replaced in the holster, between the collection of the gallery and some of the probes, possibly causing device orientation differences between gallery and probe.
- Experiment 4 (Same day, Pocket, With repositioning): For this experiment, the gallery is from activity 13 of the first session and the probes are from activities 13, 14, and 15 of the first session. Due to repositioning of the phone between activities we expect changes in device orientation as in experiment 3.
- Experiment 5 (Cross day, Holster, With repositioning): For this experiment, the gallery is from activity 16 of the first session and the probes are from activities 16, 17, and 18 of the second session. This involves a few days separation between gallery and probe data collection and changes several covariates such as clothing, footwear and phone orientation.
- Experiment 6 (Cross day, Pocket, With repositioning): For this experiment, the gallery is from activity 13 of the first session and the probes are from activities 13, 14, and 15 of the second session. Due to elapsed time between gallery and probe data collection similar to experiment 5, several covariates are expected to have changed. Because of placement in pocket, this experiment includes a greater variability in orientation than Experiment 5 where the phone was placed in the holster.

The EERs for the six experiments are shown in Figure 8.

Since experiments 1 and 2 involve no repositioning of the phone, the baseline EER is low (about 7%). The orientation independent methods show higher EERs (8.6% to 11%). This is because in the case of MAG valuable 3D information is lost. The other methods try to increase the match scores by alignment; the genuine matches already being aligned, do not benefit from this process but the impostor match scores are increased due to alignment.

Experiment 3 is has higher baseline EER (15.2%) than experiments 1 and 2, but relatively low compared to the remaining experiments. This is because the gallery and probe data were collected on the same day and the home location of the phone was the holster. The holster is normally placed in a nearly fixed location and orientation when the clothing does not change. At 95% confidence level the orientation independent methods produce EER (14.9% to 17.1%), similar to the baseline EER.

Experiment 4 has the higher baseline EER (20.0%) than experiment 3. Even though both experiments 3 and 4 have gallery and probes from the same day, repositioning the phone in the pocket allows a greater orientation change than repositioning in the holster. In this experiment, the benefits of the orientation independent methods are clearly apparent since they produce lower EERs (15.8% to 17.2%) than baseline within 95% confidence interval.

Muaaz and Mayrhofer [20] report same day EER of 7% on a dataset of 35 subjects with phone in pocket, using magnitude for orientation invariance. Same day EER of 16.26% on dataset of 48 subjects with phone in fixed orientation on right hip is reported in [21]. Keeping in mind that the USF-PDA dataset with 101 subjects is larger, we can conclude that the performance of our algorithm on the above 4 same day experiments is better.

Experiment 5 has baseline EER 32.6% due to the gallery and probes coming from different days. All alignment methods except KAB have EERs 30.4% to 33.3%, which is similar to the baseline EER in the 95% confidence interval. KAB has a significantly lower EER of 25.3%.

Experiment 6 has baseline EER 37.7% due to the gallery and probes coming from different days and the home location being the pocket allowing significant orientation changes. All alignment methods have EERs 24.6% to 29.0%, which is significantly lower than the baseline EER in the 95% confidence interval.

Cross day EERs of 22% to 28% are reported on a dataset of 48 subjects with the phone in a pouch attached to the hip (relatively same orientation) in [25]. Muaaz and Nickel [21] report cross day EER 29.39% on 48 subjects for normal walk with phone in pouch attached to right hip (relatively same orientation). The USF-PDA dataset with unconstrained phone placement produces comparable results in spite of having unconstrained placement.

B. USF-PDA Dataset - Different Locations

We designed two experiments to study the dependence of algorithm performance when gallery and probe signals are from different locations of the phone. That is, probes from pocket activities are compared against holster gallery and probes from holster activities are compared against pocket gallery. Similar to the same location experiments, galleries always came from activities that involved no phone action (13 or 16) from the first session for the subject. The gallery approximately corresponds to the first straight segment of the walk (see Figure 7) for these activities. The probes were formed from the remaining walking portion of activities 16 and 13 of the same session. The probe portion of the data is split into 5 second segments to generate probes. The two experiments are as follows:

- Experiment PH (Gallery Pocket, Probe Holster): For this experiment, the gallery is from activity 13, where the phone is in the pocket and the probes are from activity 16, where the phone is in the holster.

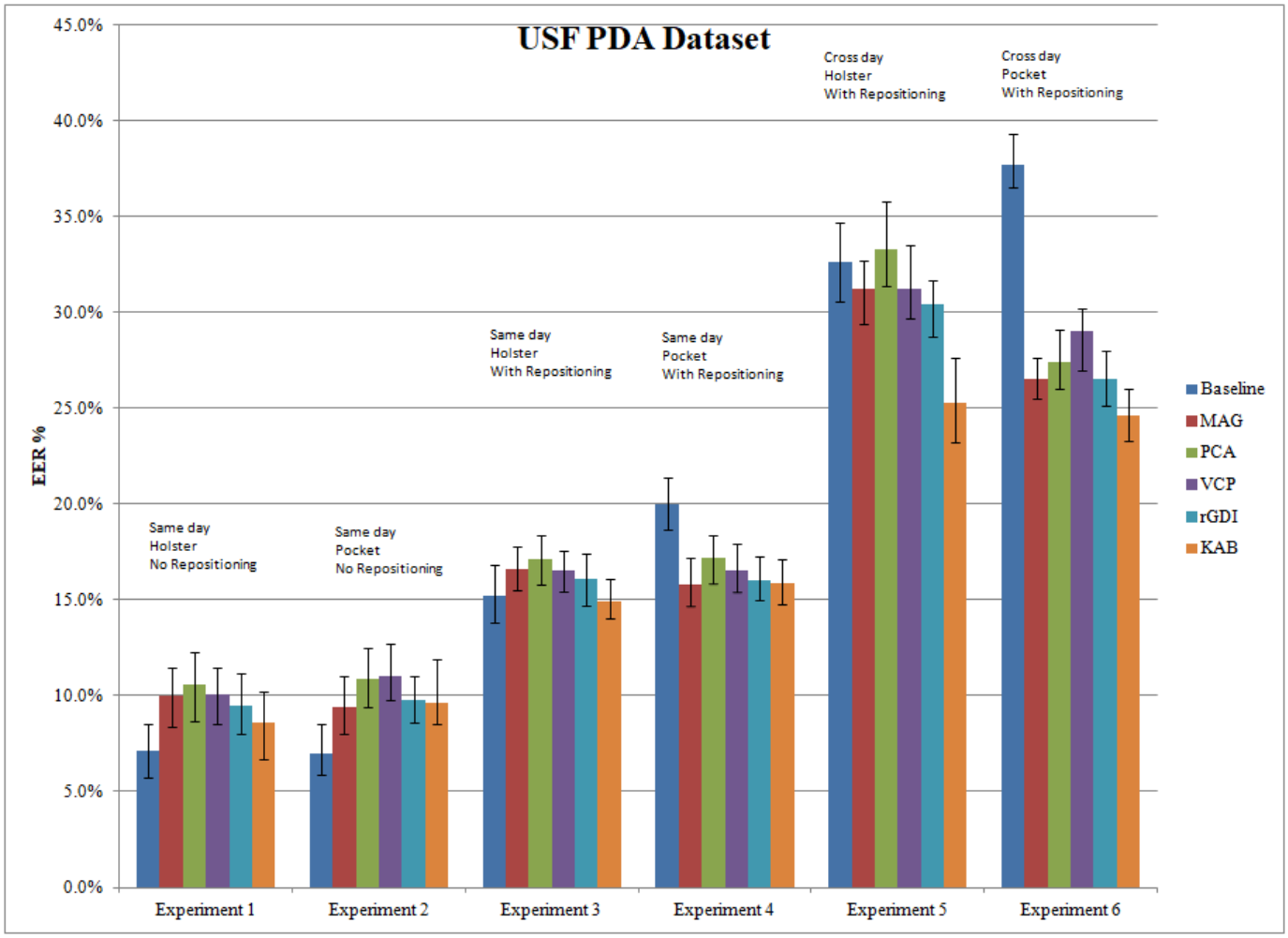

Fig. 8. The EER% along with the 95% confidence interval error bars for the baseline and five orientation independent methods of the six experiments on the USF-PDA dataset are shown here. Experiments 1 and 2 do not involve repositioning of the phone, hence all the orientation independent methods produce higher EER's compared to the baseline. Experiment 3, even though it involves repositioning, it is on the same day and in holster. This has almost the same effect as no repositioning. The results are similar to experiments 1 and 2. Experiment 4 is same day in pocket. This results in orientation changes as shown in higher baseline EER compared to experiments 1, 2 and 3. The orientation independent methods lower the EER considerably. Experiments 5 and 6 are cross day and have the highest baseline EERs. In these two experiments, the KAB method provides the most reduction in EER.

TABLE III
EER OF THE ROTATION INVARIANT METHODS ON EXPERIMENTS WITH GALLERY AND PROBE USING DIFFERENT PHONE LOCATIONS

Gallery/Probes	Baseline	MAG	PCA	VCP	rGDI	KAB
Pocket/Holster	47.9	46.6	42.2	39.8	45.3	38.4
Holster/Pocket	47.0	43.1	39.5	36.6	43.5	34.9

- Experiment HP (Gallery Holster, Probe Pocket): For this experiment, the gallery is from activity 16, where the phone is in the holster and the probes are from activity 13, where the phone is in the pocket.

The results of experiments with gallery and probe from different phone locations are presented in Table III. The baseline EERs are high in the 47% to 48% range. All the orientation independent methods improve the performance to varying extents, with the method based on Kabsch alignment giving the best result in both experiments. The performance of both the baseline method and the orientation independent methods are considerably worse than the any of the experiments where gallery and probe were from the same phone location, including the cross day experiments. This is explained by the fact the gait dynamics measured at the hip (holster) and the thigh (pocket) have different characteristics. For instance the hip undergoes a significant rotation about the vertical axis. This rotation is negligible in the thigh region. Similarly the thigh experiences a swinging motion in the front/back direction. This motion is not significant in the hip. One solution to address different placements of the phone would be to generate a gallery with signals from all possible phone locations. During matching, the probe can be compared to all the signals in the gallery or limited number of them if the phone location can be narrowed down based on the probe signal.

C. OU-ISIR-2 Dataset

In this evaluation we use only the level walk from all 3 IMUZs in the second subset. Only the 483 subjects that had data across all 3 IMUZs are considered.

Since there are 2 sessions and 3 IMUZ sensors, the first session of each sensor was used as the gallery against

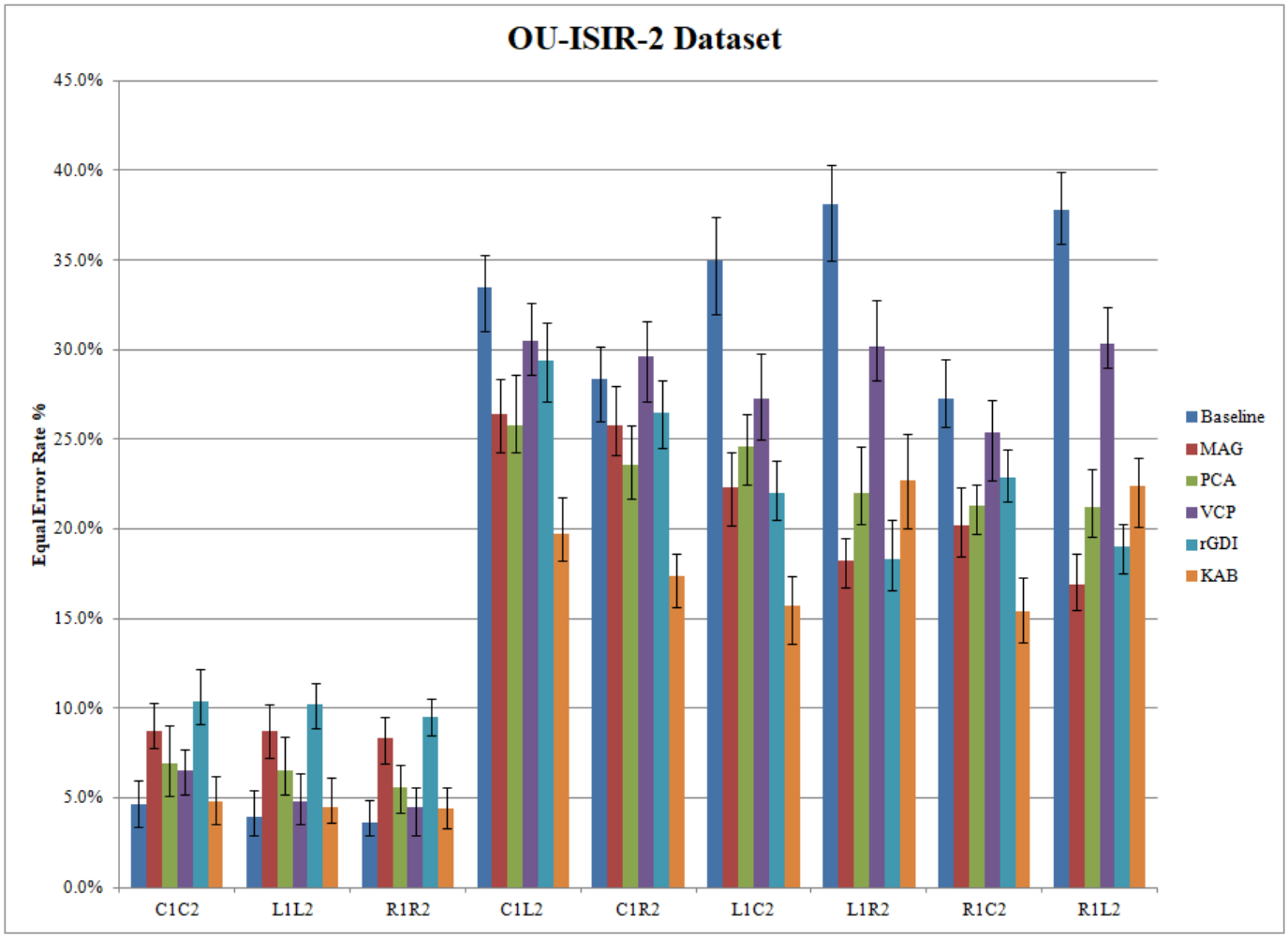

Fig. 9. The EER% along with the 95% confidence interval error bars for the baseline and five orientation independent methods of the nine experiments on the OU-ISIR-2 dataset are shown here. Experiments 1, 2 and 3 use sensors in same orientation for gallery and probe, hence all the orientation independent methods produce higher EER's compared to the baseline. Experiments 4 through 9 use sensors with different orientations for gallery and probe. This results in higher baseline EER compared to experiments 1, 2 and 3. In most of these experiments the orientation independent methods lower the EER considerably.

the second session of each sensor as probe, resulting in 9 experiments (C1C2, L1L2, R1R2, C1L2, C1R2, L1C2, L1R2, R1C2 and R1L2). For example the experiment C1L2 stands for gallery from Center sensor session 1 and probe from Left sensor session 2.

The results of the experiments are shown in Figure 9. In a similar manner to the USF-PDA dataset, the 3 experiments C1C2, L1L2 and R1R2 where the gallery and probes are from the same sensor (there is no change in orientation), the baseline EERs are low 3.6% to 4.6%. The alignment methods produce EERs in the range 4.4% to 10.4% which are equal to or higher than the baseline. In the remaining six experiments that involve sensor/orientation change between the gallery and probes, the effects of alignment is clearly visible. The baseline average EER for the 6 experiments is 33.4%. The 4 alignment methods (MAG, PCA, VCP, rGDI) other than KAB produce average EERs of 21.6%, 23.1%, 28.9%and 23.0% respectively. The average EER due the KAB method is 18.9%. When there is an orientation change, all alignment methods produce lower EERs than the baseline EER to 95% confidence.

D. OU-ISIR-1 Dataset

In contrast to the OU-ISIR-2 dataset, this dataset contains data only from the center IMUZ sensor, but from 745 subjects. Due to the fixed sensor location and orientation, this dataset is not ideal to evaluate the orientation methods. But results from other research are available for comparing the algorithm framework. Hence we compare only the baseline and Kabsch alignment results against other results in Figure 10. The results presented are based on using only the accelerometer signals.

Method B1 presented in [4] uses the magnitude of the accelerometer signal. Cycle detection is done by finding minima of error measure between a sliding sample of the signal and the entire signal. Gallery cycles are created after discarding outliers based on Dynamic Time Warping (DTW). The gallery and probe are matched using L1-norm based Cyclic

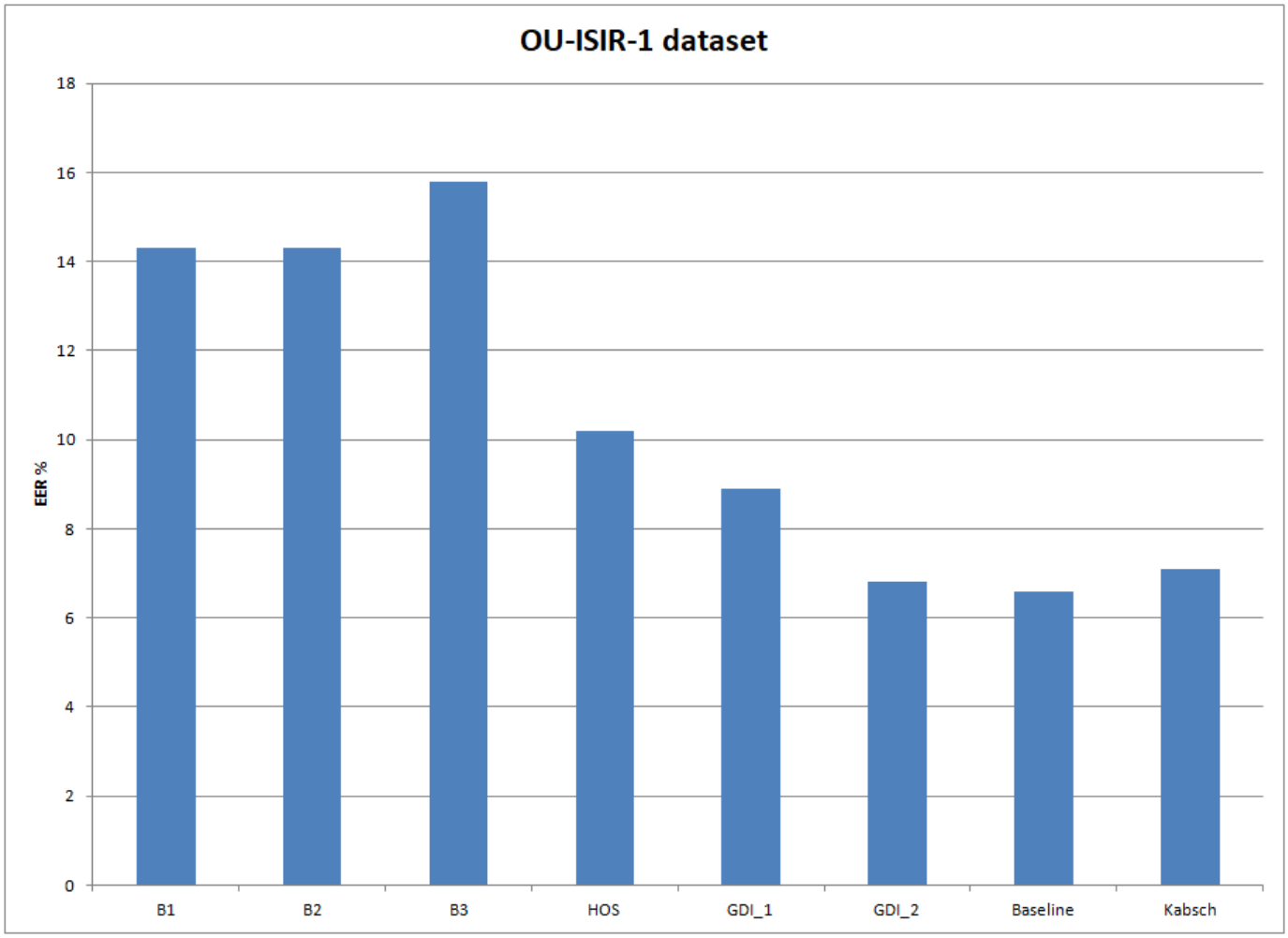

Fig. 10. The performance of our algorithm relative to other published algorithms on the OU-ISIR-1 dataset are presented here. Methods B1, B2 and B3 are implementations of methods presented respectively in [4], [29] and [6] by Ngo *et al.* in [22]. HOS is method based on Higher Order Statistics presented in [35]. GDI_1 and GDI_2 are methods based on Gait Dynamics Image presented in [47]. Baseline is our method without alignment, Kabsch is our method with Kabsch alignment.

Rotation Metric (CRM) and DTW. Method B2 presented in [29] does cycle splitting using zero-crossing points. Matching is done using Nearest Neighbor (1-NN) based on DTW distance. Method B3 presented in [6] uses vertical component of the acceleration to detect cycles. Matching is done using L2-norm. Results shown are from [22] based on their own implementation of the above methods.

The method based on Higher Order Statistics (HOS) is described in [35]. It uses frame based segmentation. Features are based on Higher Order Cumulants (HOC). Since there is a high degree of correlation between the features, reduction is achieved using truncated Singular Value Decomposition (tSVD). Matching is done by means of correlation distance as a distance measure.

The GDI_1 and GDI_2 methods are from [47]. This approach is also frame based. Orientation invariant features called Gait Dynamics Images (GDI) are generated from the frames as described in Section IV-B.4. The GDIs are converted into i-vectors which are used as features. Matching is done using inner product (GDI_1) and cosine similarity (GDI_2).

The results of our overall framework are comparable to that of the GDI based methods and significantly better than the rest. The lack of orientation problem in this dataset is confirmed by similar results from the baseline method and Kabsch method in our framework. Based on this we can conclude that the better results from our framework are due to the better performance of our cycle splitting algorithm.

VII. Discussion and Conclusions

Biometrics have been widely used for protection of personal devices only in the past decade or so. This is a result of many factors including proliferation of a variety of devices and applications that need to be protected and the availability of robust and cost effective sensors to acquire biometric data. Biometrics such as fingerprints and face recognition have progressively reached their current maturity and wide adaptation as a result of decades of research and improvement of techniques. Compared to these, behavioral biometrics are relatively new and provide interesting opportunities for further research and improvement.

Even at the current stage of maturity inertial gait based authentication appears to be practical in selected contexts. The Equal Error Rates on several of the same day experiments are well below 10%. Keeping in mind that this represents just one operating point, systems can be designed to operate with lower false acceptance rate for applications focusing on higher security or with a lower false reject rate for enhancing user convenience.

The cross day performance is relatively poor compared to same day performance due to several factors. This is true of almost all behavioral biometric modalities. This opens up opportunities to identify the responsible factors and find solutions. This would expand the domain of applicability of inertial gait for authentication purposes.

Uncontrolled in device orientation is a significant problem in achieving acceptable authentication performance using inertial sensors. In this work we considered five different methods that make the authentication process orientation independent. When there is an actual change in orientation these methods perform 13% to 23% better than the baseline where no effort is made to address the issue. Of the five methods considered, the KAB method based on the Kabsch alignment provided the most increase in performance when there was an orientation change and the least deterioration when there was little or no orientation change.

ACKNOWLEDGMENT

The authors would like to thank the Air Force Research Laboratory and the Defense Advanced Research Project (DARPA) for the USF-PDA Data which was collected using funding under contract FA8750-13-C-0265. The views, opinions and/or findings contained in this work should not be interpreted as the official views and policies of the Department of Defense of the US Government.

Parts of the methods described in this paper are in U.S. Patent No. 9,877,668 "Orientation invariant gait matching." Sudeep Sarkar, Ravichandran Subramanian, and Miguel A. Labrador.

The authors are also grateful to Yagi Lab of The Institute of Scientific and Industrial Research (ISIR), Osaka University for sharing their valuable inertial sensor data.

REFERENCES

[1] H. J. Ailisto, M. Lindholm, J. Mantyjarvi, E. Vildjiounaite, and S.-M. Makela, "Identifying people from gait pattern with accelerometers," *Proc. SPIE*, vol. 5779, pp. 7–14, Apr. 2005.

[2] G. Cola, M. Avvenuti, A. Vecchio, G.-Z. Yang, and B. Lo, "An unsupervised approach for gait-based authentication," in *Proc. IEEE 12th Int. Conf. Wearable Implantable Body Sensor Netw. (BSN)*, Jun. 2015, pp. 1–6.

[3] O. Dehzangi, M. Taherisadr, and R. ChangalVala, "IMU-based gait recognition using convolutional neural networks and multi-sensor fusion," *Sensors*, vol. 17, no. 12, p. 2735, 2017.

[4] M. O. Derawi, P. Bours, and K. Holien, "Improved cycle detection for accelerometer based gait authentication," in *Proc. IEEE Int. Conf. Intell. Inf. Hiding Multimedia Signal Process.*, Oct. 2010, pp. 312–317.

[5] J. Frank, S. Mannor, J. Pineau, and D. Precup, "Time series analysis using geometric template matching," *IEEE Trans. Pattern Anal. Mach. Intell.*, vol. 35, no. 3, pp. 740–754, Mar. 2013.

[6] D. Gafurov, E. Snekkenes, and P. Bours, "Improved gait recognition performance using cycle matching," in *Proc. Int. Conf. Adv. Inf. Netw. Appl. Workshops*, Apr. 2010, pp. 836–841.

[7] T. Hoang, D. Choi, and T. Nguyen, "On the instability of sensor orientation in gait verification on mobile phone," in *Proc. 12th Int. Joint Conf. e-Bus. Telecommun. (ICETE)*, vol. 4, Jul. 2015, pp. 148–159.

[8] T. Hoang, D. Choi, V. Vo, A. Nguyen, and T. Nguyen, "A lightweight gait authentication on mobile phone regardless of installation error," in *Proc. IFIP Int. Inf. Secur. Conf.* Berlin, Germany: Springer, 2013, pp. 83–101.

[9] M. Hofmann, J. Geiger, S. Bachmann, B. Schuller, and G. Rigoll, "The TUM gait from audio, image and depth (GAID) database: Multimodal recognition of subjects and traits," *J. Vis. Commun. Image Represent.*, vol. 25, no. 1, pp. 195–206, Jan. 2014.

[10] T. Iso and K. Yamazaki, "Gait analyzer based on a cell phone with a single three-axis accelerometer," in *Proc. ACM Conf. Human-Comput. Interaction Mobile Devices Services*, 2006, pp. 141–144.

[11] H. Iwama, M. Okumura, Y. Makihara, and Y. Yagi, "The OU-ISIR gait database comprising the large population dataset and performance evaluation of gait recognition," *IEEE Trans. Inf. Forensics Security*, vol. 7, no. 5, pp. 1511–1521, Oct. 2012.

[12] M. Juhola, Y. Zhang, and J. Rasku, "Biometric verification of a subject through eye movements," *Comput. Biol. Med.*, vol. 43, no. 1, pp. 42–50, Jan. 2013.

[13] W. Kabsch, "A discussion of the solution for the best rotation to relate two sets of vectors," *Acta Crystallographica Sect. A, Cryst. Phys., Diffraction, Theor. General Crystallogr.*, vol. 34, no. 5, pp. 827–828, Sep. 1978.

[14] A. Kale, N. Cuntoor, B. Yegnanarayana, A. N. Rajagopalan, and R. Chellappa, "Gait analysis for human identification," in *Proc. Int. Conf. Audio-Video-Based Biometric Pers. Authentication*. Springer, 2003, pp. 706–714.

[15] T. Kobayashi, K. Hasida, and N. Otsu, "Rotation invariant feature extraction from 3-D acceleration signals," in *Proc. IEEE Int. Conf. Acoust., Speech Signal Process.*, May 2011, pp. 3684–3687.

[16] J. Mantyjarvi, M. Lindholm, E. Vildjiounaite, S.-M. Makela, and H. A. Ailisto, "Identifying users of portable devices from gait pattern with accelerometers," in *Proc. IEEE Int. Conf. Acoust., Speech, Signal Process.*, vol. 2, Mar. 2005, pp. 973–976.

[17] D. S. Matovski, M. S. Nixon, S. Mahmoodi, and J. N. Carter, "The effect of time on gait recognition performance," *IEEE Trans. Inf. Forensics Security*, vol. 7, no. 2, pp. 543–552, Apr. 2012.

[18] S. P. Moustakidis, J. B. Theocharis, and G. Giakas, "Subject recognition based on ground reaction force measurements of gait signals," *IEEE Trans. Syst., Man, Cybern. B, Cybern.*, vol. 38, no. 6, pp. 1476–1485, Dec. 2008.

[19] S. P. Moustakidis, J. B. Theocharis, and G. Giakas, "Feature extraction based on a fuzzy complementary criterion for gait recognition using GRF signals," in *Proc. 17th Mediterranean Conf. Control Autom.*, Jun. 2009, pp. 1456–1461.

[20] M. Muaaz and R. Mayrhofer, "Orientation independent cell phone based gait authentication," in *Proc. 12th Int. Conf. Adv. Mobile Comput. Multimedia*, 2014, pp. 161–164.

[21] M. Muaaz and C. Nickel, "Influence of different walking speeds and surfaces on accelerometer-based biometric gait recognition," in *Proc. 35th Int. Conf. Telecommun. Signal Process. (TSP)*, Jul. 2012, pp. 508–512.

[22] T. T. Ngo, Y. Makihara, H. Nagahara, Y. Mukaigawa, and Y. Yagi, "The largest inertial sensor-based gait database and performance evaluation of gait-based personal authentication," *Pattern Recognit.*, vol. 47, no. 1, pp. 228–237, 2014.

[23] T. T. Ngo, Y. Makihara, H. Nagahara, Y. Mukaigawa, and Y. Yagi, "Orientation-compensative signal registration for owner authentication using an accelerometer," *IEICE Trans. Inf. Syst.*, vol. 97, no. 3, pp. 541–553, 2014.

[24] K.-T. Nguyen, T.-L. Vo-Tran, D.-T. Dinh, and M.-T. Tran, "Gait recognition with multi-region size convolutional neural network for authentication with wearable sensors," in *Proc. Int. Conf. Future Data Secur. Eng.* Cham, Switzerland: Springer, 2017, pp. 197–212.

[25] C. Nickel, M. O. Derawi, P. Bours, and C. Busch, "Scenario test of accelerometer-based biometric gait recognition," in *Proc. 3rd Int. Workshop Secur. Commun. Netw. (IWSCN)*, May 2011, pp. 15–21.

[26] G. Pan, Y. Zhang, and Z. Wu, "Accelerometer-based gait recognition via voting by signature points," *Electron. Lett.*, vol. 45, no. 22, pp. 1116–1118, Oct. 2009.

[27] I. Papavasileiou, S. Smith, J. Bi, and S. Han, "Gait-based continuous authentication using multimodal learning," in *Proc. IEEE/ACM Int. Conf. Connected Health, Appl., Syst. Eng. Technol. (CHASE)*, Jul. 2017, pp. 290–291.

[28] V. Patel, R. Chellappa, D. Chandra, and B. Barbello, "Continuous user authentication on mobile devices: Recent progress and remaining challenges," *IEEE Signal Process. Mag.*, vol. 33, no. 4, pp. 49–61, Jul. 2016.
[29] L. Rong, Z. Jianzhong, L. Ming, and H. Xiangfeng, "A wearable acceleration sensor system for gait recognition," in *Proc. IEEE Conf. Ind. Electron. Appl.*, May 2007, pp. 2654–2659.
[30] S. Sarkar, P. J. Phillips, Z. Liu, I. R. Vega, P. Grother, and K. W. Bowyer, "The humanID gait challenge problem: Data sets, performance, and analysis," *IEEE Trans. Pattern Anal. Mach. Intell.*, vol. 27, no. 2, pp. 162–177, Feb. 2005.
[31] S. Sarkar, R. Subramanian, and Z. Liu, "Gait recognition: Evaluation," in *Encyclopedia of Biometrics*, S. Z. Li and A. K. Jain, Eds. New York, NY, USA: Springer, 2014, pp. 1–12.
[32] J. Shelton, J. Adams, D. Leflore, and G. Dozier, "Mouse tracking, behavioral biometrics, and GEFE," in *Proc. IEEE Southeastcon*, Apr. 2013, pp. 1–6.
[33] J. D. Shutler, M. G. Grant, M. S. Nixon, and J. N. Carter, "On a large sequence-based human gait database," in *Applications and Science in Soft Computing*. Berlin, Germany: Springer, 2004, pp. 339–346.
[34] H. Sobral *et al.*, "Human gait analysis using instrumented shoes," in *Proc. IEEE 4th Portuguese Meeting Bioeng. (ENBENG)*, Feb. 2015, p. 1.
[35] S. Sprager and M. B. Juric, "An efficient HOS-based gait authentication of accelerometer data," *IEEE Trans. Inf. Forensics Security*, vol. 10, no. 7, pp. 1486–1498, Jul. 2015.
[36] S. Sprager and M. B. Juric, "Inertial sensor-based gait recognition: A review," *IEEE Sensors J.*, vol. 15, no. 9, pp. 22089–22127, Sep. 2015.
[37] R. Subramanian *et al.*, "Orientation invariant gait matching algorithm based on the Kabsch alignment," in *Proc. IEEE Int. Conf. Identity, Secur. Behav. Anal. (ISBA)*, Mar. 2015, pp. 1–8.
[38] J. Suutala and J. Röning, "Methods for person identification on a pressure-sensitive floor: Experiments with multiple classifiers and reject option," *Inf. Fusion*, vol. 9, no. 1, pp. 21–40, Jan. 2008.
[39] D. Tan, K. Huang, S. Yu, and T. Tan, "Efficient night gait recognition based on template matching," in *Proc. 18th Int. Conf. Pattern Recognit. (ICPR)*, vol. 3, Aug. 2006, pp. 1000–1003.
[40] P. S. Teh, A. B. J. Teoh, and S. Yue, "A survey of keystroke dynamics biometrics," *Sci. World J.*, vol. 2013, Aug. 2013, Art. no. 408280.
[41] R. Vera-Rodriguez, R. P. Lewis, J. S. D. Mason, and N. W. D. Evans, "A large scale footstep database for biometric studies created using cross-biometrics for labelling," in *Proc. 10th Int. Conf. Control, Autom., Robot. Vis.*, Dec. 2008, pp. 1361–1366.
[42] W. Xu, Y. Shen, Y. Zhang, N. Bergmann, and W. Hu, "Gait-watch: A context-aware authentication system for smart watch based on gait recognition," in *Proc. 2nd Int. Conf. Internet-Things Design Implement. (IoTDI)*, New York, NY, USA, Apr. 2017, pp. 59–70.
[43] Z.-M. Yao, X. Zhou, E.-D. Lin, S. Xu, and Y.-N. Sun, "A novel biometrie recognition system based on ground reaction force measurements of continuous gait," in *Proc. 3rd Int. Conf. Human Syst. Interaction*, May 2010, pp. 452–458.
[44] S. Yu, D. Tan, and T. Tan, "A framework for evaluating the effect of view angle, clothing and carrying condition on gait recognition," in *Proc. 18th Int. Conf. Pattern Recognit. (ICPR)*, vol. 4, 2006, pp. 441–444.
[45] J. Yun, "User identification using gait patterns on UbiFloorII," *Sensors*, vol. 11, no. 3, pp. 2611–2639, 2011.
[46] Z. Yuting, P. Gang, K. Jia, M. Lu, Y. Wang, and Z. Wu, "Accelerometer-based gait recognition by sparse representation of signature points with clusters," *IEEE Trans. Cybern.*, vol. 45, no. 9, pp. 1864–1875, Sep. 2015.
[47] Y. Zhong and Y. Deng, "Sensor orientation invariant mobile gait biometrics," in *Proc. IEEE Int. Joint Conf. Biometrics*, Sep./Oct. 2014, pp. 1–8.

Ravichandran Subramanian received the B.Tech. degree in mechanical engineering from IIT Madras, India, and the master's degree in computer science from the University of South Florida, Tampa, FL, USA. He is currently enrolled in the Doctoral Program with the Department of Computer Science and Engineering, University of South Florida. He is a Senior Principal Engineer with the Security and Detection Systems Division, L3 Technologies. His research interests include biometrics, image processing, computer vision, and machine learning.

Sudeep Sarkar (F'13) received the M.S. and Ph.D. degrees in electrical engineering from The Ohio State University. He is currently a Professor and Chair of Computer Science and Engineering and an Associate Vice President of I-Corps Programs with the University of South Florida, Tampa. He has 25-year expertise in computer vision and pattern recognition algorithms and systems, holds six U.S. patents, licensed technologies, and has published high-impact journal and conference papers. He is a fellow and a member of the Board of Directors of the National Academy of Inventors. He was a recipient of the National Science Foundation CAREER Award in 1994, the USF Teaching Incentive Program Award for Undergraduate Teaching Excellence in 1997, the Outstanding Undergraduate Teaching Award in 1998, and the Ashford Distinguished Scholar Award in 2004, and the University Presidential Fellowship. He is a fellow of the American Association for the Advancement of Science, the International Association for Pattern Recognition, and the American Institute for Medical and Biological Engineering. He has served on many journal boards and is currently the Editor-in-Chief of *Pattern Recognition Letters*.